Collaborative Spectrum Sensing via Online Estimation of Hidden Bivariate Markov Models

Yuandao Sun, *Student Member, IEEE*, Brian L. Mark, *Senior Member, IEEE*, and Yariv Ephraim, *Fellow, IEEE*

***Abstract*— Collaborative spectrum sensing exploits multiuser diversity by combining spectrum sensing information from multiple secondary users to make joint decisions about spectrum occupancy. In hard fusion schemes, each secondary user makes a hard decision on spectrum occupancy and a fusion center makes a final decision by combining the individual hard decisions according to a fusion rule. In soft fusion schemes, each secondary user provides a signal power measurement to the fusion center, which performs further processing on the collection of all observations to make a final decision. In this paper, we propose hard and soft fusion collaborative spectrum sensing schemes based on the online hidden bivariate Markov chain modeling of the signals received by secondary users. Compared with prior collaborative sensing schemes, the proposed model-based schemes do not rely on precomputed thresholds or weights, and achieve superior performance. The online estimation of hidden bivariate Markov models provides predictive information that can be used to improve the performance of the dynamic spectrum access. Numerical results are presented to demonstrate the performance and communication overhead tradeoffs of the proposed collaborative spectrum sensing schemes.**

***Index Terms*— Cognitive radio, spectrum sensing, collaboration, hidden Markov model, online recursive estimation.**

I. Introduction

COGNITIVE radio has been proposed as a promising technology for reclaiming underutilized spectrum resources to satisfy the increasing demand for more wireless spectrum. In dynamic spectrum access networks, unlicensed or secondary users (SUs) are permitted to make use of portions of a licensed spectrum band that are left idle by the licensed or primary users (PUs) as long as they do not cause harmful interference to the PUs. In such a scenario, the SUs are equipped with cognitive radios that can detect spectrum holes and make use of such holes for their own communications. Spectrum holes can be characterized in space, frequency, and time, or a combination thereof. In this paper, we focus on temporal spectrum sensing of a given channel, where the PU occupying the channel alternates between an active and an idle state [1]–[3]. The duty cycle and statistical behavior of the PU is unknown and may vary on a slow time-scale. A group of SUs collaborate in estimating the time intervals for which the channel is idle. Note that temporal spectrum sensing is not necessary for detecting TV white spaces, for TV broadcast signals are known to be active with nearly 100% duty cycle. In these situations, spatial spectrum sensing [4] or wideband spectrum sensing techniques [5] are more appropriate. For bursting PU signals, however, such sensing techniques are prone to detection error, particular for low duty cycle signals or low signal-to-noise ratio scenarios. The paging channel studied in [2] provides an example of a bursting PU signal which admits temporal opportunities for dynamic spectrum access. Temporal sensing can also be combined with spatial and/or wideband spectrum sensing techniques [6], [7].

Various approaches to temporal spectrum sensing have been studied in the literature, including energy detection, matched filter detection, and cyclostationary detection (cf. [8]). Matched filter detection requires knowledge of the modulation scheme employed by the PU. Cyclostationary detection can achieve better performance than energy detection, but is much more computationally intensive and requires longer sensing times. In [2], an approach to temporal spectrum sensing based on a hidden bivariate Markov model (HBMM) was proposed. The HBMM extends the more traditional hidden Markov model (HMM) by allowing for more general state sojourn time distributions of the PU. The state sojourn times of an HBMM have discrete phase-type distributions, whereas those of an HMM are limited to geometric distributions. The higher degrees of freedom afforded by the HBMM can provide higher modeling fidelity than the HMM, which results in better performance. Recently, a recursive parameter estimation algorithm for the HBMM, based on Rydén's [9] recursive algorithm for the HMM, was developed in [10]. Together with the state estimation and prediction recursions presented in [2], the recursive HBMM parameter estimation algorithm forms the basis for a fully online temporal spectrum sensing scheme.

Manuscript received September 18, 2015; revised January 13, 2016 and April 7, 2016; accepted April 10, 2016. Date of publication April 27, 2016; date of current version August 10, 2016. This work was supported in part by the U.S. National Science Foundation (NSF) through the Division of Computing and Communication Foundations under Grant CCF-0916568 and in part by U.S. NSF through the Division of Computer and Network Systems under Grant CNS-1205453 and Grant CNS-1421869. The associate editor coordinating the review of this paper and approving it for publication was H. Wymeersch.

Y. Sun was with the Department of Electrical and Computer Engineering, George Mason University, Fairfax, VA 22030 USA. He is now with Deloitte Consulting LLP (e-mail: ysun12@gmu.edu).

B. L. Mark and Y. Ephraim are with the Department of Electrical and Computer Engineering, George Mason University, Fairfax, VA 22030 USA (e-mail: bmark@gmu.edu; yephraim@gmu.edu).

Color versions of one or more of the figures in this paper are available online at http://ieeexplore.ieee.org.

Digital Object Identifier 10.1109/TWC.2016.2558506

1536-1276 © 2016 IEEE. Personal use is permitted, but republication/redistribution requires IEEE permission.
See http://www.ieee.org/publications_standards/publications/rights/index.html for more information.

In radio environments with severe shadowing and fading effects, spectrum sensing by a single SU can lead to hidden terminal effects and other errors which can result in harmful interference to the PUs. Collaborative spectrum sensing techniques leverage multiuser diversity to improve sensing performance, particularly in severely shadowed environments with hidden terminals. Collaborative sensing involves multiple SUs in a joint decision-making process to determine when a given channel is idle or active [11]. Collaborative sensing schemes can be categorized into two main types: hard fusion and soft fusion.

In hard fusion schemes, each SU makes an independent decision on the state of the PU in a given time slot. The 1-bit decisions from a group of SUs are forwarded to a fusion center, which combines the individual SU decisions into a final decision for the state of the PU according to a fusion rule. Hard fusion based on a majority voting rule is one of the simplest suboptimal collaboration methods [12]. Majority voting is a special case of a linear hard fusion rule, in which a linear combination of the 1-bit decisions from the SUs is compared to a threshold to obtain the final decision. In [13], a more sophisticated hard fusion scheme is studied, which takes the sensing throughput and the sensing time into account. In this scheme, the 1-bit hard decisions are combined linearly with weights that are precomputed based on the likelihood ratio test (LRT) (cf. [14]). The differences in the reliability of the 1-bit decisions made by different SUs are reflected in the weights of the decisions at the fusion center. However, the global optimum solution for the threshold of the fusion rule and weights for SUs is more difficult to obtain than in soft fusion schemes.

In soft fusion schemes, each SU forwards received signal power measurements to the fusion center, which then processes all of the measurements to estimate the state of the PU. A popular class of soft fusion schemes computes a linear combination of the measurements from the SUs according to a set of weights, which is then compared to a threshold to obtain the final decision. Linear soft fusion generally outperforms hard fusion schemes in terms of detection accuracy, but the weights and threshold for soft fusion must be chosen appropriately, and the computational and communication overhead tends to be much higher. In [15], a "softened" hard fusion scheme with 2-bit communication overhead per SU is proposed to achieve a good tradeoff between detection accuracy and communication overhead. However, the weights for linear combining are computed offline. In [16], a linear soft fusion scheme is proposed in which the optimal threshold and weights are determined jointly by optimizing a so-called modified deflection coefficient, which characterizes the probability distribution function of the global test statistic at the fusion center. This approach has significantly lower computational complexity compared to LRT-based linear soft fusion, yet achieves comparable performance.

In this paper, we develop hard and soft fusion collaborative sensing schemes based on online hidden bivariate Markov chain modeling of the temporal dynamics of the PU as well as the wireless channel conditions. Our approach relies on the online parameter estimation algorithm for the single channel temporal spectrum sensing approach presented in [10]. As in [2] and [10], the detector frontend for each SU is assumed to provide averaged power estimates obtained from received signal power measurements, and the channel follows a path loss model with lognormal shadowing. In our proposed soft fusion scheme, the averaged power estimates from the SUs are quantized and transmitted to the fusion center. Using the vector of quantized power estimates from the SUs, an estimate of the parameter of a hidden bivariate Markov model is computed recursively and used to estimate the state of the PU. In our HBMM hard fusion scheme, each SU computes a hard decision on the active/idle state of the PU based on the observed signal power measurements and an estimate of the associated HBMM parameter as in [10]. The hard decisions from the SUs are transmitted to the fusion center, which then applies linear combining to obtain the final decision.

Our numerical results show that the HBMM soft fusion scheme achieves significantly better performance than linear soft fusion schemes, e.g., [13], [16]. Linear soft fusion schemes typically require prior knowledge of channel parameters to precompute the weights for linear combination and the decision threshold. Thus, they are not able to adapt to changes in the channel conditions. In a preliminary version of our work [17], we showed how online HBMM parameter estimation could be applied to compute the weights and threshold for linear soft fusion in an online manner. However, the HBMM soft fusion scheme developed here obviates the need for linear soft fusion altogether. The HBMM hard fusion scheme performs nearly as well as linear soft fusion, with much lower bandwidth overhead, provided the HBMM parameter used by each SU for state estimation is relatively accurate. Such parameter could be estimated offline by means of a training sequence. Alternatively, a compromise between spectrum sensing accuracy and communication overhead could be achieved by a hybrid scheme which employs HBMM soft fusion to obtain a good HBMM parameter estimate and then switches to HBMM hard fusion for PU state detection. A further benefit of the HBMM approaches to collaborative spectrum sensing is that they provide predictive information on the PU state which can be leveraged to reduce harmful interference to PU and improve spectrum utilization.

The remainder of the paper is organized as follows. In Section II, we discuss the system model for collaborative sensing. In Section III, we review the HBMM and online estimation of the HBMM. In Section IV, we develop online HBMM soft and hard fusion schemes for collaborative spectrum sensing. In Section V, we present numerical results to evaluate the performance of the proposed collaborative sensing schemes. In Section VI, we provide concluding remarks.

II. System Model for Collaborative Sensing

We consider a system consisting of one PU transmitting on a given narrowband channel and Q SUs performing collaborative spectrum sensing. The PU alternates between an active state, in which a signal of fixed power is transmitted over the narrowband channel, and an idle state, in which no signal is transmitted. We denote the idle state of the PU

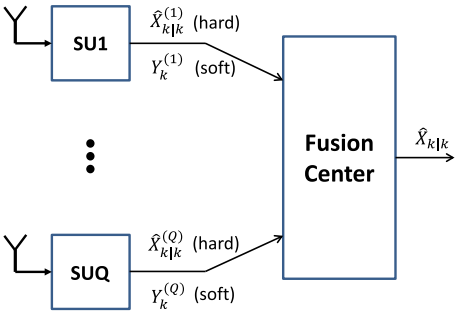

Fig. 1. A generic collaborative sensing scheme.

at time $k\Delta$ by $X_k = 1$, and the active state by $X_k = 2$, where Δ is a sampling period.[1] The transmitted signal goes through a fading channel with additive white Gaussian noise. The wireless propagation environment is assumed to be governed by a standard path loss with lognormal shadowing model [19, pp. 40–41]. We ignore fast fading since it can be reduced effectively by an averaging filter (cf. [20]). Let $u(t)$ denote the complex baseband demodulated PU signal. For a particular SU, let $c(t)$ denote a random process representing the fading, and let $w(t)$ denote the additive thermal noise of the receiver. The signal received by the SU is given by $y(t) = c(t)u(t) + w(t)$. The received baseband signal may be envisioned as a phasor perturbed by the additive noise. The received signal is sampled every Δ seconds, and each sample is represented by the logarithm of its power.

Let Y_k denote the logarithm of the power of the kth sample of the received signal of the SU. Given the state $X_k = a$ of the PU, the samples $\{Y_k\}$ are assumed statistically independent, and each Y_k is assumed normally distributed with some mean μ_a and variance σ_a^2. This normal model is motivated by the central limit theorem [21]. The relation between $\{\mu_a, \sigma_a^2\}$ and the parameters of the fading additive noise channel is non-trivial. In [21, Corollary 5.6.3], the statistics of the logarithm of the smoothed periodogram of a stationary process with small dependence span, were studied. The power of the baseband demodulated PU signal may be seen as a value of the smoothed periodogram of a broadband process measured at a particular frequency. It was shown that the log-smoothed-periodogram at a given frequency is asymptotically normal with mean that depends on the underlying power spectral density, and a constant variance that is independent of the underlying power spectral density. In our model we allow both the mean and variance of each Y_k to depend on the state of the PU, and hence on the underlying power of the received signal, in order to accommodate possible deviations from the model of [21]. If the variance of Y_k is somewhat independent of the underlying hypothesis, then that will be reflected in its estimated values. We shall use $Y_k^{(q)}$ and $X_k^{(q)}$ to denote Y_k and X_k, respectively, from the qth SU.

A block diagram of a generic collaborative sensing scheme is shown in Fig. 1. In soft fusion, at each time k, the SUs transmit quantized versions of their received signals $Y_k^{(1)}, \ldots, Y_k^{(q)}$, to the fusion center, where they are used to predict the state of the PU at time $k+\tau$ for some nonnegative integer τ. The state estimator is denoted by $\hat{X}_{k+\tau|k}$ and takes values in $\mathbb{X} = \{1, 2\}$. For conventional fusion schemes that do not have predictive capability, $\tau = 0$. In a *linear* soft fusion scheme, a weighted sum, $V_k = \sum_{q=1}^{Q} w_q Y_k^{(q)}$, of the observations at time k is computed and compared to a threshold ψ as follows [13], [15], [16]:

$$\hat{X}_{k|k} = \begin{cases} 1, & V_k < \psi, \\ 2, & V_k \geq \psi, \end{cases} \tag{1}$$

where $w_1, \ldots w_Q$ are the weights. Typically, the threshold and weights for soft fusion are computed offline [15], [16].

In [16], an approach to computing the weights for linear soft fusion was proposed, based on maximizing a so-called modified deflection coefficient (MDC). Numerical results showed that this approach achieved near-optimal performance for linear soft fusion. Let $\boldsymbol{w} = (w_1, \ldots, w_Q)$ denote the vector of weights. Let $\mu_a^{(q)}$ and $\sigma_a^{(q)}$ denote, respectively, the conditional mean and standard deviation of $Y_k^{(q)}$ given $X_k^{(q)} = a$, for the qth SU. Define $\boldsymbol{\mu}_a = (\mu_a^{(q)} : q = 1, \ldots, Q)$ for $a \in \mathbb{X}$. Let $\boldsymbol{Y}_k = (Y_k^{(1)}, \ldots, Y_k^{(Q)})$ denote the *vector* observation sample at time k. The channels observed by the Q SUs are assumed to be conditionally independent given the PU state. Under this assumption, the conditional covariance matrix of $\boldsymbol{Y}_k$ given $X_k^{(q)} = a$ is given by $\Sigma_a = \text{diag}([\sigma_a^{(q)}]^2 : q = 1, \ldots, Q)$. Then the optimal MDC weight vector derived in [16] is given by

$$\boldsymbol{w} = \frac{\Sigma_2^{-1}\boldsymbol{\mu}'}{\|\Sigma_2^{-1}\boldsymbol{\mu}'\|_2}, \tag{2}$$

where $\boldsymbol{\mu} = \boldsymbol{\mu}_2 - \boldsymbol{\mu}_1$ and $'$ denotes matrix transpose. In Section V, we compare the performance of the proposed HBMM soft fusion scheme against linear soft fusion based on (2). The HBMM soft fusion approach is not restricted to linear estimation, and the state of the PU is estimated from current and previous observations from all SUs.

In a hard fusion scheme, at each time k, each SUq makes an independent decision, $X_{k|k}^{(q)}$, on the PU state based on the observations $Y_1^{(q)}, \ldots, Y_k^{(q)}$. The 1-bit SU hard decisions are transmitted to the fusion center, which computes a final decision, denoted by $\hat{X}_{k|k}$, according to a hard fusion rule. For example, the "OR" rule decides that the PU is active, i.e., state 2, if at least one of the SU hard decisions has the value 2. The "majority voting" rule decides that the PU is active if more than half of the Q SU hard decisions have value 2. The OR-rule and majority voting rule are special cases of the q-out-of-Q rule, where $1 \leq q \leq Q$ is an integer constant. Here, the PU state is determined to be active if q or more of the hard decisions are 'active'; otherwise, the PU state is determined to be idle. The OR and majority voting rules are equivalent to the q-out-of-Q rule when $q = 1$ and $q = \lfloor Q/2 \rfloor$, respectively. The q-out-of-Q fusion rule is in turn a special case of linear hard fusion (cf. [13]). Under linear combining, the decision variable is computed as

[1] In this paper, we follow the convention, common in the HMM literature, in which states are numbered starting from 1, see, e.g., [9], [18].

$V_k = \sum_{q=1}^{Q} w_q \hat{X}_{k|k}^{(q)}$, where the w_q are predetermined weights. The decision variable V_k is then compared to a threshold ψ to obtain the final decision $\hat{X}_{k|k}$ as in (1). The q-out-of-Q fusion rule is a special case of linear hard fusion.

In conventional hard fusion schemes, each SU employs an energy detector to obtain a hard decision at each time k, i.e., SUq estimates the PU state as follows:

$$\hat{X}_{k|k}^{(q)} = \begin{cases} 1, & Y_k^{(q)} < \psi_q, \\ 2, & Y_k^{(q)} \geq \psi_q, \end{cases} \tag{3}$$

where ψ_q denotes a threshold, which is usually computed offline. Typically, a majority voting rule is applied at the fusion center. In the HBMM hard fusion scheme, the state estimate $\hat{X}_{k|k}^{(q)}$ for each SUq is a function of the current and all previous observations, not just the current sample $Y_k^{(q)}$. In addition, the HBMM hard fusion scheme employs a linear fusion rule based on the MDC weight vector given by (2).

III. Hidden Bivariate Markov Model

A. Definition and Parametrization

An HBMM is a trivariate process (Y, X, S), where Y denotes an observable process with continuous alphabet, and the underlying process, $Z = (X, S)$, is a finite-state bivariate Markov chain. In [10], HBMM was adopted to model the temporal spectrum sensing for a single SU. Here, Y is used to represent the received signal power at an SU and X represents the state of the PU. The process S is introduced so that the sojourn time of the process X in each state $a \in \{1, 2\}$ takes on a discrete-time phase-type distribution [2].

For a general HBMM, we denote the state-space of X by $\mathbb{X} = \{1, \ldots, d\}$, the state-space of S by $\mathbb{S} = \{1, \ldots, r\}$, and we let $\mathbb{Z} = \mathbb{X} \times \mathbb{S}$ denote the state-space of Z. The processes Y and S are assumed to be conditionally independent given X. Let $f(y_k; \theta_a)$ denote the conditional density of Y_k given $X_k = a$ at time k, where θ_a is a parameter depending on $a \in \mathbb{X}$. From our received signal model assumptions, $f(y_k; \theta_a)$ is a Gaussian density and we set $\theta_a = (\mu_a, \sigma_a)$ to be the mean and standard deviation of this density. The initial distribution of Z is denoted by a $1 \times dr$ row vector $\pi = [\pi_{ai} : (a, i) \in \mathbb{Z}]$, where $\pi_{ai} = P(Z_1 = (a, i))$. The transition matrix of Z is denoted by a $dr \times dr$ matrix $G = [g_{ab}(ij) : (a, i), (b, j) \in \mathbb{Z}]$, where $g_{ab}(ij) = P(Z_k = (b, j) \mid Z_{k-1} = (a, i))$.

The parameter of the HBMM is given by (π, θ, G). In practice, however, the effect of the initial probability distribution π on the Markov chain fades quickly and accurate estimation of it is not necessary. Therefore, we assume the HBMM parameter to be $\phi = (\theta, G)$. The total number of elements in ϕ is $L = 2d + d^2r^2$. We write $\phi = [\phi_\ell : \ell = 1, \ldots, L]$, where ϕ_ℓ denotes the ℓth element of ϕ under a given ordering scheme. Let $\Phi \subseteq \mathbb{R}^L$ denote the space of feasible HBMM parameters. We note that when $r = 1$, the HBMM reduces to the traditional HMM, where the state sojourn time distributions are geometric.

B. Online Parameter Estimation

The online HBMM parameter estimation algorithm developed in [10] is based on an algorithm for the HMM developed by Rydén [9], and a recursion for computing the score function for an HMM from Lystig and Hughes [22] (see also Willy *et al.* [23]). The parameter estimation algorithm operates on a block of m observations at a time. The nth observation block is denoted by $y_{(n-1)m+1}^{nm} = \{y_{(n-1)m+1}, \ldots, y_{nm}\}$. For convenience, the first observation block, y_1^m, is denoted simply by y^m. With a slight abuse of notation, let ϕ_n denote the nth HBMM parameter estimate computed by the online algorithm upon receiving the nth observation block. The recursion for ϕ_n is given by

$$\phi_{n+1} = \Pi_{\mathcal{G}} \left[\phi_n + \gamma_n \chi \left(y_{nm+1}^{(n+1)m}; \phi_n \right) \right], \tag{4}$$

$n = 0, 1, 2, \ldots$, where $\Pi_{\mathcal{G}}$ denotes a projection operator mapping the estimate into a compact, convex set $\mathcal{G} \subseteq \Phi$, and $\chi \left(y_{nm+1}^{(n+1)m}; \phi_n \right)$ is the score function with respect to the parameter ϕ_n applied to the $(n+1)$st observation block. The sequence $\{\gamma_n\}$ consists of positive step sizes γ_n that decrease to zero as $n \to \infty$ to enable convergence of the stochastic approximation algorithm (4). We adopt from [9], $\gamma_n = \gamma_0 n^{-\epsilon}$ for some $\gamma_0 > 0$, $\epsilon \in (0.5, 1]$, and $n = 1, 2, \ldots$.

The score function for the first observation block, y^m, is given as follows:

$$\begin{aligned} \chi(y^m; \phi) &= \frac{\partial \log p_\phi(y^m)}{\partial \phi} \\ &= \sum_{(b,j) \in \mathbb{Z}} \frac{1}{p_\phi(y^m)} \frac{\partial}{\partial \phi} p_\phi(y^m, z_m = (b, j)), \end{aligned} \tag{5}$$

where $p_\phi(y^m)$ denotes the joint density of the observation block y^m. Under some mild assumptions, Rydén proved that for HMMs, the sequence $\{\phi_n\}$ converges to a point lying in the set of Kuhn-Tucker points for minimizing the Kullback-Leibler divergence with respect to the true parameter defined over $\mathcal{G}$. As discussed in [10], Rydén's convergence results carry over to the HBMM.

The summands in (5) can be organized into a $dr \times L$ matrix $H_m(y^m; \phi)$ such that each row corresponds to one state (b, j) and each column corresponds to one component of the parameter ϕ. The score function can then be obtained from

$$\chi(y^m; \phi) = \mathbf{1}' H_m(y^m; \phi), \tag{6}$$

where $\mathbf{1}$ denotes a column vector of all ones. It was shown in [10] that the matrix $H_m(y^m; \phi)$. can be computed recursively as follows, starting from the initial condition $H_0(y^0; \phi) = \mathbf{0}$, where $\mathbf{0}$ denotes a $dr \times L$ zero matrix:

$$\begin{aligned} H_k(y^k; \phi) = \frac{1}{c_k} \Big\{ & F(y_k)' H_{k-1}(y^{k-1}; \phi) \\ & + (I \otimes \xi_{k-1}) \frac{\partial}{\partial \phi} [\text{vec } F(y_k)]' \Big\}, \end{aligned} \tag{7}$$

for $k = 1, \ldots, m$, where I denotes the identity matrix of order dr, $\otimes$ denotes the Kronecker product, the $dr \times dr$ matrix $F(y_k)$ is given by

$$F(y_k) = [f_{ij}^{ab}(y_k; \theta_b) : (a, i), (b, j) \in \mathbb{Z}], \tag{8}$$

with $f_{ij}^{ab}(y_k; \theta_b) = g_{ab}(ij) f(y_k; \theta_b)$, and vec $F(y_k)$ in (7) denotes the column vector obtained by stacking the columns

of the matrix $F(y_k)$ one on top of the other. The elements of the Jacobian matrix $\partial[\text{vec } F(y_k)]'/\partial\theta$ are partial derivatives of $f_{ij}^{ab}(y_k;\theta_b)$. The $1 \times dr$ row vector ξ_k and scalar c_k are given by

$$\xi_k = \frac{1}{c_k}\xi_{k-1}F(y_k), \quad c_k = \xi_{k-1}F(y_k)\mathbf{1}, \tag{9}$$

for $k = 1, 2, \ldots$, with the initial condition $\xi_0 = \pi$.

C. State Recursion

The estimate of the parameter ϕ can be applied to calculate a forward recursion for the conditional state probabilities given the observation sequence. Define the $dr \times dr$ block diagonal matrix $B(y_k)$, with its diagonal blocks given by $\{p(y_k \mid X_k = a)I,\ a \in \mathbb{X}\}$, for $k = 1, 2, \ldots$, where I is an $r \times r$ identity matrix. Then the scaled forward recursion for $\bar{\alpha}(z_k, y^k) = p_\phi(z_k \mid y^k)$ is given by (cf. [10, eq. (5)])

$$\bar{\alpha}_1 = \frac{\pi B(y_1)}{c_1}, \quad \bar{\alpha}_k = \frac{\bar{\alpha}_{k-1}GB(y_k)}{c_k}, \quad k = 2, 3, \ldots, \tag{10}$$

where $c_1 = \pi B(y_1)\mathbf{1}$, and $c_k = \bar{\alpha}_{k-1}GB(y_k)\mathbf{1}$.

The conditional probability of the bivariate state at time $k+\tau$ given the observations up to and including time k can then be computed as follows (cf. [2, eq. (22)]):

$$\begin{aligned} p_\phi(z_{k+\tau} \mid y^k) &= \sum_{z_k \in \mathbb{Z}} p_\phi(z_k \mid y^k)\ p_\phi(z_{k+\tau} \mid z_k) \\ &= \sum_{z_k \in \mathbb{Z}} \bar{\alpha}(z_k, y^k)\left[G^\tau\right]_{z_k, z_{k+\tau}}. \end{aligned} \tag{11}$$

A detection scheme for the state of the PU at time $k+\tau$ given the received signal power y^k is specified by (cf. [2, eq. (23)]):

$$\hat{X}_{k+\tau|k} = \begin{cases} 1, & \sum_s p_\phi(z_{k+\tau} = (1, s) \mid y^k) \geq \eta, \\ 2, & \text{otherwise}, \end{cases} \tag{12}$$

for $k = 1, 2, \ldots$, where η is a decision threshold, $0 < \eta < 1$. The detection scheme is a maximum a posteriori (MAP) detector when $\eta = 0.5$. When $\tau = 0$, $\hat{X}_{k+\tau|k} = \hat{X}_{k|k}$ is an estimate of the current state X_k. When $\tau = 1, 2, \ldots$, $\hat{X}_{k+\tau|k}$ is the τ-step predicted estimate of the state $X_{k+\tau}$. The current and predicted state estimates $\hat{X}_{k+\tau|k}$ can be directly applied to make dynamic spectrum access decisions.

IV. Model-Based Collaborative Spectrum Sensing

In this section, we develop soft and hard fusion schemes for collaborative spectrum sensing by expanding upon the online HBMM estimation approach summarized in Section III.

A. HBMM Soft Fusion

Referring to Fig. 2, at each time k, the observation sample $Y_k^{(q)}$ from each SUq is transmitted directly to the fusion center, which forms the vector observation sample $\boldsymbol{Y}_k = (Y_k^{(1)}, \ldots, Y_k^{(Q)})$. The proposed soft fusion scheme is based on hidden bivariate Markov chain modeling of the *vector* observation sequence $\boldsymbol{Y} = \{\boldsymbol{Y}_k; k = 1, 2, \ldots\}$ generated by the Q SUs. Here, the conditional output density parameter is given

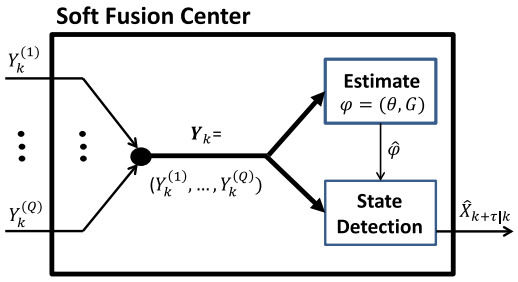

Fig. 2. HBMM soft fusion.

by $\boldsymbol{\theta} = (\boldsymbol{\theta}_a : a \in \mathbb{X})$, where $\boldsymbol{\theta}_a = (\theta_a^{(1)}, \ldots, \theta_a^{(Q)})$, and $\theta_a^{(q)}$ is the conditional output density parameter of each SUq when the PU is in state a. With this definition of $\boldsymbol{\theta}$, the parameter of the HBMM is given formally by $\phi = (\boldsymbol{\theta}, G)$, which we also denote by $\phi = [\phi_\ell : \ell = 1, \ldots, L]$, where $L = 2dQ + d^2r^2$.

Recursions for online parameter and state estimation of the HBMM in the setup of Fig. 2 with vector observation input can be obtained from those given in Section III, by replacing the scalar sequence y^k by the vector sequence $\boldsymbol{y}^k$ and θ by $\boldsymbol{\theta}$. To compute $f(\boldsymbol{y}_k; \boldsymbol{\theta}_b)$, we assume that the Q cognitive radio channels are conditionally independent given the state of the PU, in which case, $f(\boldsymbol{y}_k; \boldsymbol{\theta}_b) = f(y_k^{(1)}; \theta_b^{(1)}) \cdot f(y_k^{(2)}; \theta_b^{(2)}) \cdots f(y_k^{(Q)}; \theta_b^{(Q)})$. The elements of the $d^2r^2 \times L$ Jacobian matrix $\partial[\text{vec } F(\boldsymbol{y}_k)]'/\partial\phi$ are given as follows:

$$\begin{aligned} \frac{\partial}{\partial[g_{ce}(\iota l)]} f_{ij}^{ab}(\boldsymbol{y}_k; \boldsymbol{\theta}_b) &= f(\boldsymbol{y}_k; \boldsymbol{\theta}_b)\ \mathbf{1}_{\{(c,\iota)=(a,i),(e,l)=(b,j)\}}, \\ \frac{\partial}{\partial(\mu_c^{(q)})} f_{ij}^{ab}(\boldsymbol{y}_k; \boldsymbol{\theta}_b) &= f_{ij}^{ab}(\boldsymbol{y}_k; \boldsymbol{\theta}_b)\frac{y_k^{(q)} - \mu_b^{(q)}}{(\sigma_b^{(q)})^2}\ \mathbf{1}_{\{c=b\}}, \\ \frac{\partial}{\partial(\sigma_c^{(q)})} f_{ij}^{ab}(\boldsymbol{y}_k; \boldsymbol{\theta}_b) &= f_{ij}^{ab}(\boldsymbol{y}_k; \boldsymbol{\theta}_b) \\ &\quad \cdot \frac{(y_k^{(q)} - \mu_b^{(q)})^2 - (\sigma_b^{(q)})^2}{(\sigma_b^{(q)})^3}\ \mathbf{1}_{\{c=b\}}, \end{aligned} \tag{13}$$

for $(c, \iota), (e, l) \in \mathbb{Z}$, where $\mathbf{1}_A$ denotes an indicator function on the set or condition A. When the state recursion (10) is generalized for vector observation input, the matrix $B(y_k)$ is replaced by the $dr \times dr$ block diagonal matrix $B(\boldsymbol{y}_k) = B(y_k^{(1)}) \cdot B(y_k^{(2)}) \cdots B(y_k^{(Q)})$, where $B(y_k^{(q)})$ is a $dr \times dr$ block diagonal matrix with diagonal blocks given by $\{p(y_k^{(q)} \mid X_k = a)I,\ a \in \mathbb{X}\}$, for $k = 1, 2, \ldots$. The product form of $B(\boldsymbol{y}_k)$ follows from assuming conditional independence of the cognitive radio channels given the state of the PU.

The complexity of the HBMM soft fusion scheme in each time slot is dominated by the computation of $H_m(\boldsymbol{y}^m; \phi)$, which requires $O(d^3r^3 \cdot (2dQ + d^2r^2)) = O(d^4r^3Q + d^5r^5) = O(r^3Q + r^5)$ when $d = 2$. Since Q is a small constant in practice, the overall complexity of the proposed soft fusion scheme is essentially the same as that of the hard fusion scheme. If the linear combination weights and decision threshold are precomputed, the complexity of soft linear fusion becomes only $O(Q)$. However, if these parameters are estimated online using HBMM parameter estimation, as

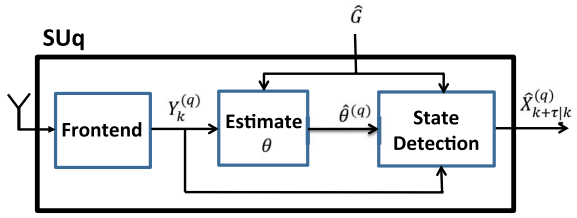

Fig. 3. Block diagram of SU for HBMM hard fusion.

proposed in [17], the complexity of the online soft linear fusion scheme per time slot becomes $O(r^5)$. In practice, small values of r in the range 2 to 5 are sufficient to represent the PU active/idle sojourn time distributions accurately (see [2]).

B. HBMM Hard Fusion

The main advantage of hard fusion schemes relative to soft fusion schemes is the low bandwidth overhead due to the transmission of a 1-bit by each SU to the fusion center. However, the local decision made by an individual SU may not always be reliable, for example, when the received signal at the SU has undergone severe shadowing. Incorporating an HBMM to model the dynamics of the PU and the wireless propagation environment, can lead to much better performance under such conditions.

The architecture of each SUq cognitive radio transceiver in our proposed hard fusion scheme is depicted in Fig. 3. In this scheme, the online HBMM parameter estimation algorithm of Section III-B is decoupled into two parts: 1) estimating the transition matrix G, and 2) estimating the parameter $\theta^{(q)}$ of the conditional output distribution for each SUq. The rationale for separating the two blocks is that estimation of θ is significantly easier than that of the transition matrix. The estimate of G can either be computed locally, based on the final decisions fed back to each SU from the fusion center, or it could be computed by the fusion center and broadcast to all SUs. Both options are equivalent with respect to estimation of G. The estimates of G are provided as input to the conditional output parameter estimation block. The transition matrix estimates are updated less frequently than the sensing decisions, so a small delay in the feedback loop from the fusion center to the SUs will not adversely affect the overall performance of the scheme.

Consider first the conditional output density parameter estimation block for the qth SU. To simplify notation, we shall drop the superscript (q) in the following discussion. The parameter of interest, $\theta = (\theta_a : a \in \mathbb{X})$, can be estimated in a block-recursive manner using (4) with θ replacing ϕ, where the score function is a $1 \times 2d$ row vector given by (6), and $H_m(y^m; \theta)$ in (6) can be computed recursively using (7). In this case, the elements of the $d^2r^2 \times 2d$ Jacobian matrix $\partial[\text{vec } F(y_k)]'/\partial\theta$ are given as follows:

$$\frac{\partial f_{ij}^{ab}(y_k;\theta_b)}{\partial \mu_c} = f_{ij}^{ab}(y_k;\theta_b) \cdot \frac{y_k - \mu_b}{\sigma_b^2} \mathbf{1}_{\{c=b\}},$$
$$\frac{\partial f_{ij}^{ab}(y_k;\theta_b)}{\partial \sigma_c} = f_{ij}^{ab}(y_k;\theta_b) \cdot \frac{(y_k - \mu_b)^2 - \sigma_b^2}{\sigma_b^3} \mathbf{1}_{\{c=b\}}, \quad (14)$$

for $c \in \mathbb{X}$.

Estimation of G is also performed using the recursive algorithm of Section III-B. Since in estimating G, the observation data comes from the final decisions of the fusion center, the observable process Y in the recursive algorithm may be taken to be X, with values in the state-space $\mathbb{X}$, i.e., the HBMM reduces to a bivariate Markov chain. Here, the parameter $G = [g_{ab}(ij) : (a,i),(b,j) \in \mathbb{Z}]$ is estimated by using (4), (5), and (7), but with $f_{ij}^{ab}(y_k;\theta_b)$ in (8) given as follows:

$$f_{ij}^{ab}(y_k;\theta_b) = g_{ab}(ij) f(y_k;\theta_b) = g_{ab}(ij)\, \mathbf{1}_{\{y_k=b\}}. \quad (15)$$

In addition, the elements of the $d^2r^2 \times d^2r^2$ Jacobian matrix $\partial[\text{vec } F(y_{(k)})]'/\partial G$ in (7) are given as follows:

$$\frac{\partial f_{ij}^{ab}(y_k;\theta_b)}{\partial [g_{ce}(\imath l)]} = \mathbf{1}_{\{y_k=b,(c,\imath)=(a,i),(e,l)=(b,j)\}}, \quad (16)$$

for $(c,\imath),(e,l) \in \mathbb{Z}$.

Each SU computes a local estimate of the PU state based on the observation data and HBMM parameter estimate. The mean and standard deviation for the conditional density is updated after each block of observation data. Since the HBMM parameter $\phi = (\theta, G)$ is estimated online, an estimate of the state at time k, as well as a predicted estimate at time $k+\tau$, where $\tau > 0$, can be computed. The state detection scheme for the qth decision block is given formally by (12), dropping the superscript in the notation for $\hat{X}_{k+\tau|k}^{(q)}$. The local SU decisions are sent to the fusion center, which then makes a final decision on the state of the PU at time k via a fusion rules. In our numerical experiments, the best performance was achieved when a linear fusion rule of the form (1) was used, with weights determined according to (2).

The complexity of the conditional output density estimation block in each time slot is dominated by the computation of $H_m(y^m;\theta)$, which requires $O(d^3r^3 \cdot 2d) = O(d^4r^3)$ arithmetic operations. The computation of the transition matrix estimation block is dominated by the computation of $H_m(y^m; G)$, which requires $O(d^3r^3 \cdot d^2r^2) = O(d^5r^5)$ arithmetic operations. Given the parameter $\phi = (\theta, G)$, the state detection scheme has complexity $O(d^2r^2)$ [2]. Therefore, the computational complexity for each SU is $O(d^5r^5) = O(r^5)$, when $d = 2$. Since linear fusion has complexity $O(Q)$, the overall complexity of HBMM hard fusion is given by $O(r^5 + Q)$ per time slot, which in practice reduces to $O(r^5)$.

V. Numerical Results

The performance of the proposed hard and soft fusion spectrum sensing schemes were evaluated using simulation in MATLAB and compared with the linear soft fusion scheme of [16].

A. Simulation Setup

For the online parameter estimation algorithm given in (4), we set $\gamma_n = \gamma_0 n^{-\varepsilon}$ with $\gamma_0 = 0.3$ and $\varepsilon = 0.35$. We set the block size $m = 20$. The parameter space $\mathcal{G}$ and projection operator $\Pi_{\mathcal{G}}$ in (4) are the same in [10]. To improve the convergence speed and stability, a warmup period is introduced to provide a good initial estimate for the conditional output

TABLE I
MEAN AND STANDARD DEVIATION OF CONDITIONAL DENSITIES FOR SCENARIO 1

	$(\mu_1^{(q)}, \sigma_1^{(q)})$	$(\mu_2^{(q)}, \sigma_2^{(q)})$
SU1	(-105.00,6.32)	(-88.00,8.94)
SU2	(-100.00,5.91)	(-86.00,8.36)
SU3	(-103.00,6.71)	(-98.00,8.06)

mean and standard deviation vectors for both of the proposed collaborative sensing schemes. We use a sequence y^{n_0} of length $n_0 = 200$ to establish the initial parameter value using the following initialization procedure:

1) Let $\mathbb{A}_1 = \{k \in \{1, \ldots, n_0\} : y_k < (\max(y^{n_0}) + \min(y^{n_0}))/2\}$ and $\mathbb{A}_2 = \{1, \ldots, n_0\} \backslash \mathbb{A}_1$, where $\backslash$ denotes set-theoretic subtraction.
2) The initial estimates $\theta_a^s = (\mu_a^s, \sigma_a^s)$ are computed as follows:

$$\mu_a^s = \frac{1}{|\mathbb{A}_a|} \sum_{k \in \mathbb{A}_a} y_k, \quad \sigma_a^s = \sqrt{\frac{1}{|\mathbb{A}_a| - 1} \sum_{k \in \mathbb{A}_a} |y_k - \mu_a^s|^2}, \tag{17}$$

where $|\cdot|$ denotes set cardinality and $a \in \mathbb{X}$.

The probability vector π^s is initialized with a uniform distribution and the initial transition matrix estimate G^s is generated randomly.

In our experiments, we considered a collaboration model with three SUs (i.e., $Q = 3$). For the true parameter ϕ^0, the state transition matrix G^0 is specified by a 20×20 transition matrix adopted from [24], such that $d = 2$ and $r = 10$. The true transition matrix was estimated from real spectrum measurements of a paging channel collected in [25] using the Baum algorithm. For the estimation blocks we have set $d = 2$ and $r = 10$, but a smaller value of r could be used to trade off accuracy for a reduction in computational complexity. We consider two scenarios, which differ only in the parameter values associated with SU2. For scenario 1, the true mean and standard deviations of the conditional output densities for three SUs are given in the Table I. For scenario 2, all of the parameters are as in scenario 1, except that the conditional output parameters for SU2 are given as follows: $(\mu_1^{(2)}, \sigma_1^{(2)}) = (-102, 5.91)$, $(\mu_2^{(2)}, \sigma_2^{(2)}) = (-95, 8.36)$. Thus, the signal-to-noise ratio for SU2 is lower in scenario 2. In each of the simulation runs for HBMM based sensing, T observation samples are applied to estimate the HBMM parameter. The final estimate of the parameter of the HBMM is then used on a different data set of T_1 observations. This way, our testing is done in the so-called open set fashion, over-fitting of the data is avoided, and transitional parameter values of the algorithm obtained prior to its convergence are discarded. The values of T and T_1 are specified below for each set of experiments.

B. Hard Fusion

We evaluated the performance of the HBMM hard fusion scheme described in Section IV-B. From $T = 6000$ observation samples, estimates of the conditional mean and standard deviation are obtained using the estimation block in Fig. 3. The estimate of the transition matrix is computed from the sequence of hard fusion decisions. The transition matrix estimate may be computed either at the fusion center and fed back to the SUs, or locally at each SU based on the decisions fed back from the fusion center.

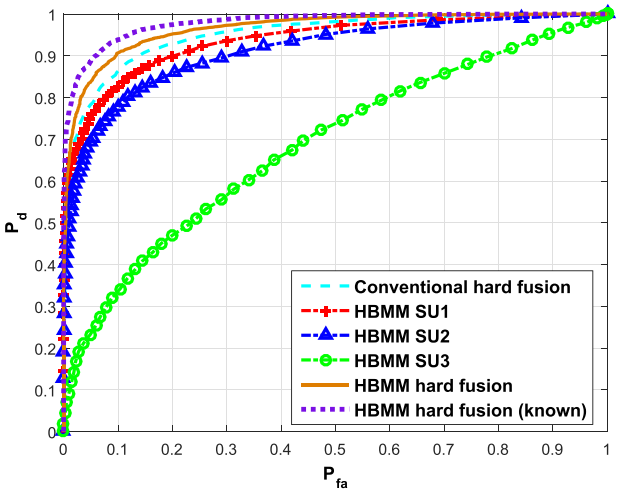

Fig. 4. ROC plot of hard fusion scheme in scenario 1.

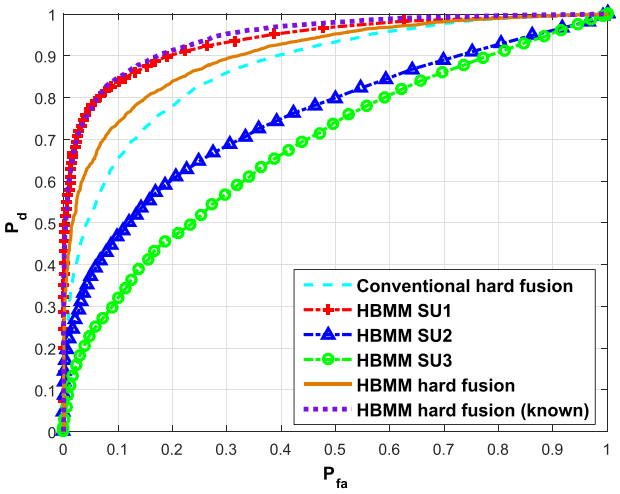

Fig. 5. ROC plot of hard fusion scheme in scenario 2.

In Figs. 4 and 5, receiver operating characteristic (ROC) curves for various detections schemes are shown, corresponding to scenarios 1 and 2, respectively. Each ROC curve is a plot of detection probability P_d vs. false alarm probability P_{fa}. For each scenario, the ROC curve labelled "HBMM hard fusion" shows the performance of the HBMM hard fusion scheme described in Section IV-B. At each SU, the estimation block in Fig. 3 is used to compute estimates of the conditional mean and standard deviation. The estimate of the transition matrix is computed based on the final hard fusion decisions. The transition matrix estimate may be computed at the fusion center and fed back to the SUs, or locally at each SU based on the decisions fed back from the fusion center. Given the HBMM parameter estimate, the ROC curve is generated by applying $T_1 = 10000$

new observation samples to the detection scheme (12) with $\tau = 0$.

In each of Figs. 4 and 5, the ROC curve labelled "HBMM hard fusion (known)" is obtained by applying the same $T_1 = 10000$ observation samples and detection scheme used to obtain the "HBMM hard fusion" curve, but with the true HBMM parameter rather than the estimate. The curve marked "Conventional hard fusion" was obtained by applying the T_1 observation samples with energy detectors at each SU and a majority voting rule at the fusion center. The curves labelled "HBMM SUq," where $q = 1, 2, 3$ show the performance of the *non-collaborative* HBMM-based spectrum sensing scheme from [10] applied to each of the SUs individually. Thus, each SU obtains a local estimate of the HBMM parameter from $T = 6000$ observation samples. Given the HBMM parameter estimate, $T_1 = 10000$ observation samples are then applied to the detection scheme (12) ($\tau = 0$) in order to generate the corresponding ROC curve.

From Fig. 4, we see that individually, SU1 and SU2 both outperform SU3 in scenario 1. In this scenario, the performance gain achieved by collaborative sensing can be seen clearly. HBMM hard fusion with known estimated parameter significantly outperforms conventional hard fusion. When the true HBMM parameter is known, the HBMM hard fusion approach to spectrum sensing achieves even better performance. The ROC performance for scenario 2 is shown in Fig. 5. From Fig. 5, we see that SU2 and SU3 have worse performance than SU1. In this case, the performance of conventional hard fusion is inferior to that of SU1, but better than that of SU2 and SU3. The performance of the HBMM hard fusion scheme is intermediate between that of conventional hard fusion and SU1. Interestingly, when the HBMM parameter is known, HBMM hard fusion performs slightly better than the non-collaborative HBMM-based sensing scheme applied at SU1.

C. Soft Fusion

We carried out simulation experiments to compare the performance of the HBMM soft and hard fusion schemes, as well as that of the near-optimal linear soft fusion scheme developed in [16]. To apply the linear soft fusion scheme, the channel parameters are assumed to be known and the weights for linear combination and the decision threshold are computed offline according to [16]. As discussed in [17], the channel parameters can be estimated online by incorporating HBMM parameter estimation, which can then be used to compute the weights and threshold for linear soft fusion in an online manner. The performance of such a scheme was found to be nearly as good as that of linear soft fusion with precomputed weights and thresholds from known channel parameters.

For scenario 1, $T = 40000$ observation samples were applied to the HBMM hard fusion, HBMM soft fusion, and linear soft fusion (with precomputed weights) schemes. A larger number of samples was used here to ensure that a sufficiently accurate estimate of the HBMM parameter could be obtained for soft fusion. The corresponding ROC curves were then computed based on $T_1 = 10000$ subsequent observation samples, and the results are shown in Fig. 6. As expected, both soft fusion schemes perform significantly better than hard fusion. The computational overhead of HBMM soft fusion is higher than that of linear soft fusion when the channel parameters are assumed known, but not significantly higher when online HBMM parameter estimation is applied to update the weights and threshold. From Fig. 6, we see that the performance of HBMM soft fusion significantly outperforms linear soft fusion. This performance gain is primarily due to fact that the linear soft fusion scheme does not take into account the temporal dynamics of the PU signal. Interestingly, in comparison to linear soft fusion, the performance of HBMM hard fusion is slightly worse when the false alarm probability $P_{\text{fa}} < 0.15$, and approximately the same when $P_{\text{fa}} > 0.15$.

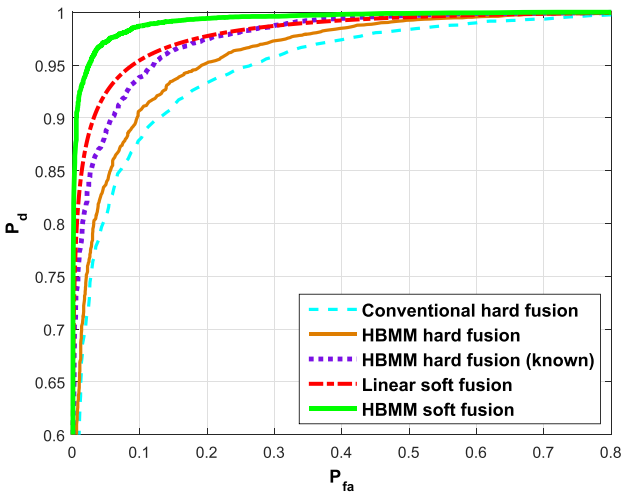

Fig. 6. ROC plot of hard and soft fusion schemes in scenario 1.

In scenario 2, the number of observation samples used for parameter estimation was increased to $T = 50000$. As before, $T_1 = 10000$ additional observation samples were applied to obtain ROC curves, which are shown in Fig. 7. As expected, the performance for each of the collaborative sensing schemes is degraded relative to that for scenario 1. The performance gap between HBMM soft fusion and linear soft fusion is larger in scenario 2 than in scenario 1. An even larger performance gap can be seen between the linear soft fusion and hard fusion schemes for the two scenarios.

D. Predictive Spectrum Sensing

A useful feature of model-based spectrum sensing is the ability to predict the future state of the PU [2], [10]. A prediction of the state at a future time could be used to augment the information provided by an estimate of the current state, thereby facilitating more proactive dynamic spectrum access. For example, even when the current state estimate indicates that the PU is idle, if the predicted state indicates that the PU will become active, an SU can vacate the channel in advance to avoid potential interference with the PU. Conversely, if the PU is detected as active in the current time

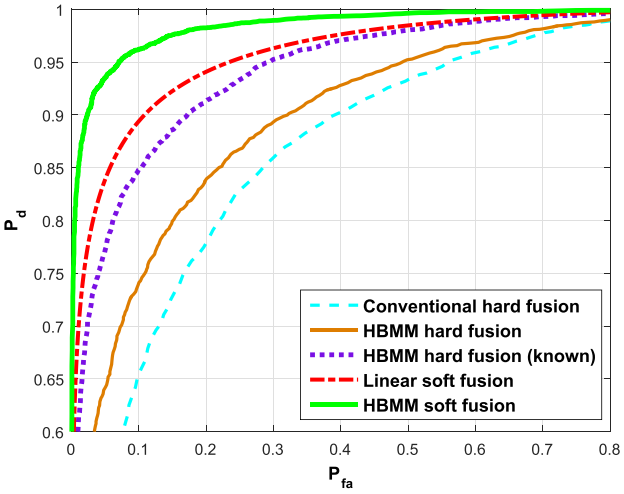

Fig. 7. ROC plot of hard and soft fusion schemes in scenario 2.

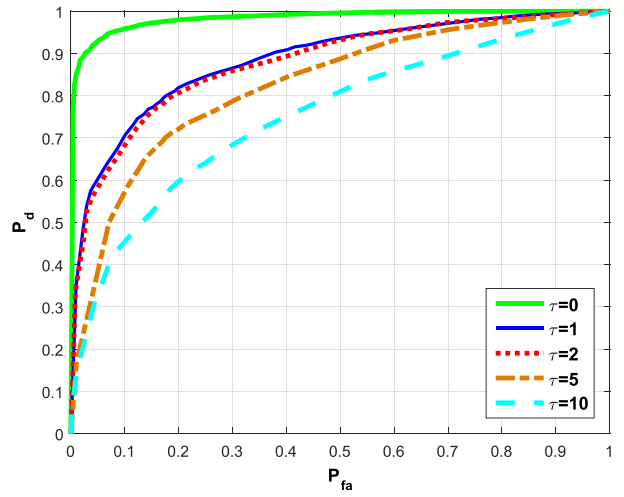

Fig. 8. τ-step HBMM soft fusion prediction performance in scenario 2.

slot but idle in a future time slot, an SU can proactively prepare for channel access in anticipation of a temporal spectrum hole. In multichannel scenarios, predictive state information can be used for selecting among multiple channels that have been detected as idle.

We ran simulation experiments to evaluate the predictive performance of the HBMM fusion scheme in scenario 2. Fig. 8 shows ROC curves for soft fusion prediction performance in scenario 2 for step sizes $\tau = 0, 1, 2, 5, 10$. Clearly, the prediction performance degrades as τ is increased. Interestingly, in this scenario the performance for $\tau = 2$ is nearly as good as for $\tau = 1$, though this does not hold in general. By comparing Figs. 7 and Fig. 8, we see that the performance of 1-step prediction is slightly better than state estimation using conventional hard fusion. The predictive performance of HBMM hard fusion, with unknown transition matrix, was rather poor, even for $\tau = 1$. However, when the transition matrix is known, the performance of HBMM hard fusion is quite close to that of HBMM soft fusion.

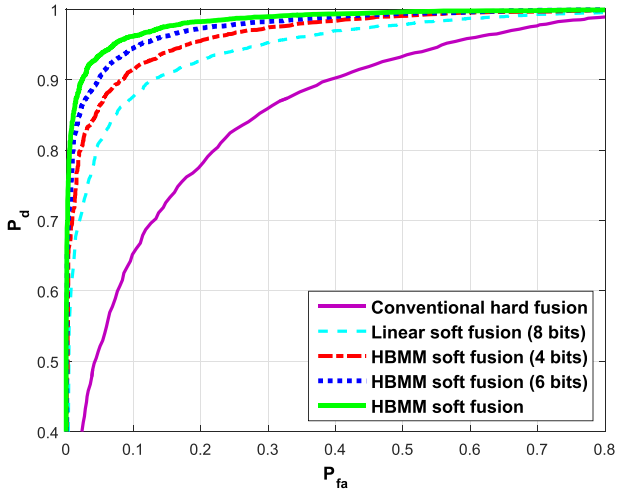

Fig. 9. ROC plot of soft decision schemes with quantization in scenario 2.

E. Coarsely Quantized Soft Fusion

The soft fusion experiments assumed a 32-bit representation of the observation samples, such that the bandwidth overhead was $32/\Delta$ bits/s, where Δ represents the time slot duration in seconds. The bandwidth overhead can be reduced, at the expense of performance, by applying coarser quantization of the observation samples. We conducted simulation experiments to evaluate the impact of coarse quantization of the observation data on the performance of the soft fusion schemes. For simplicity, we adopted a uniform quantization scheme. The quantization range for the received signal power measurements was set to $[-140, 0]$ dBm and the quantization resolution is determined by the number of bits. At each SUq, the observation sample $Y_k^{(q)}$ is quantized and encoded before being transmitted to the fusion center, which then decodes the quantized sample for further processing. In Fig. 9, ROC curves obtained for scenario 2 are shown for linear soft fusion with 8-bit samples and HBMM soft fusion with 4-bit and 6-bit samples. The degradation in performance for HBMM soft fusion can be clearly seen as the number of bits per sample is reduced from 6 to 4. We also see that HBMM soft fusion with 4-bit samples outperforms linear soft fusion with 8-bit samples. When 3-bit samples are used, the HBMM soft fusion scheme performs worse than HBMM hard fusion, and thus loses its performance advantage.

VI. Conclusion

We have developed two fully online schemes for collaborative spectrum sensing based on hidden bivariate Markov chain modeling of the received signal at the cognitive radios. In the HBMM hard fusion scheme, each SU makes an independent decision on the active/idle state of the PU and sends it to a fusion center, which applies a linear fusion rule to obtain a final decision. In the HBMM soft fusion scheme, each SU transmits an observation sample to the fusion center, which performs online parameter and state estimation of an HBMM with vector input. The hard fusion scheme incurs much lower transmission overhead than the soft fusion scheme, but has significantly poorer performance. For the soft fusion scheme, a tradeoff between transmission overhead and performance

was demonstrated by quantizing the observation data to a desired bit rate. Moreover, the model-based approach provides predictive information on the state of the PU, which can be leveraged in proactive dynamic spectrum access schemes.

Simulation results show that the HBMM soft fusion scheme achieves significantly better performance than near-optimal *linear* soft fusion schemes. The HBMM hard fusion scheme performs better than conventional hard fusion based on energy detectors, but markedly worse than linear soft fusion. When the underlying transition matrix is assumed known, the performance gap between HBMM hard fusion and linear soft fusion decreases significantly. A hybrid scheme, which employs HBMM soft fusion until a suitable estimate of the transition matrix is obtained and then switches to HBMM hard fusion, could provide another means of obtaining a suitable tradeoff between transmission overhead and detection performance.

ACKNOWLEDGMENT

The authors would like to thank the anonymous reviewers for their helpful and constructive comments.

REFERENCES

[1] K. W. Sung, S.-L. Kim, and J. Zander, "Temporal spectrum sharing based on primary user activity prediction," *IEEE Trans. Wireless Commun.*, vol. 9, no. 12, pp. 3848–3855, Dec. 2010.

[2] T. Nguyen, B. L. Mark, and Y. Ephraim, "Spectrum sensing using a hidden bivariate Markov model," *IEEE Trans. Wireless Commun.*, vol. 12, no. 9, pp. 4582–4591, Sep. 2013.

[3] A. Mariani, S. Kandeepan, and A. Giorgetti, "Periodic spectrum sensing with non-continuous primary user transmissions," *IEEE Trans. Wireless Commun.*, vol. 14, no. 3, pp. 1636–1649, Mar. 2015.

[4] B. L. Mark and A. O. Nasif, "Estimation of maximum interference-free power level for opportunistic spectrum access," *IEEE Trans. Wireless Commun.*, vol. 8, no. 5, pp. 2505–2513, May 2009.

[5] Z. Quan, S. Cui, H. V. Poor, and A. H. Sayed, "Collaborative wideband sensing for cognitive radios," *IEEE Signal Process. Mag.*, vol. 25, no. 6, pp. 60–73, Nov. 2008.

[6] T. Do and B. L. Mark, "Joint spatial–temporal spectrum sensing for cognitive radio networks," *IEEE Trans. Veh. Technol.*, vol. 59, no. 7, pp. 3480–3490, Sep. 2010.

[7] J. M. Bruno and B. L. Mark, "A recursive algorithm for joint time-frequency wideband spectrum sensing," in *Proc. WCNC Int. Workshop Smart Spectr. (IWSS)*, New Orleans, LA, USA, Mar. 2015, pp. 235–240.

[8] T. Yucek and H. Arslan, "A survey of spectrum sensing algorithms for cognitive radio applications," *IEEE Commun. Surveys Tuts.*, vol. 11, no. 1, pp. 116–130, Mar. 2009.

[9] T. Rydén, "On recursive estimation for hidden Markov models," *Stochastic Process. Appl.*, vol. 66, no. 1, pp. 79–96, Feb. 1997.

[10] Y. Sun, B. L. Mark, and Y. Ephraim, "Online parameter estimation for temporal spectrum sensing," *IEEE Trans. Wireless Commun.*, vol. 14, no. 8, pp. 4105–4114, Aug. 2015.

[11] W. Zhang, R. K. Mallik, and K. B. Letaief, "Optimization of cooperative spectrum sensing with energy detection in cognitive radio networks," *IEEE Trans. Wireless Commun.*, vol. 8, no. 12, pp. 5761–5766, Dec. 2009.

[12] V. Aalo and R. Viswanathan, "Asymptotic performance of a distributed detection system in correlated Gaussian noise," *IEEE Trans. Signal Process.*, vol. 40, no. 1, pp. 211–213, Jan. 1992.

[13] E. C. Y. Peh, Y.-C. Liang, Y. L. Guan, and Y. Zeng, "Cooperative spectrum sensing in cognitive radio networks with weighted decision fusion schemes," *IEEE Trans. Wireless Commun.*, vol. 9, no. 12, pp. 3838–3847, Dec. 2010.

[14] S. M. Kay, *Fundamentals of Statistical Signal Processing: Detection Theory*. Englewood Cliffs, NJ, USA: Prentice-Hall, 1998.

[15] J. Ma, G. Zhao, and Y. Li, "Soft combination and detection for cooperative spectrum sensing in cognitive radio networks," *IEEE Trans. Wireless Commun.*, vol. 7, no. 11, pp. 4502–4507, Nov. 2008.

[16] Z. Quan, S. Cui, and A. H. Sayed, "Optimal linear cooperation for spectrum sensing in cognitive radio networks," *IEEE J. Sel. Topics Signal Process.*, vol. 2, no. 1, pp. 28–40, Feb. 2008.

[17] Y. Sun, B. L. Mark, and Y. Ephraim, "Collaborative spectrum sensing based on hidden bivariate Markov models," in *Proc. IEEE GlobeCom Workshop Emerg. Technol. 5G Wireless Cellular Netw.*, San Diego, CA, USA, Dec. 2015, pp. 1–6.

[18] Y. Ephraim and N. Merhav, "Hidden Markov processes," *IEEE Trans. Inf. Theory*, vol. 48, no. 6, pp. 1518–1569, Jun. 2002.

[19] J. W. Mark and W. Zhuang, *Wireless Communications and Networking*. Upper Saddle River, NJ, USA: Pearson Education, Inc., 2003.

[20] B. L. Mark and A. E. Leu, "Local averaging for fast handoffs in cellular networks," *IEEE Trans. Wireless Commun.*, vol. 6, no. 3, pp. 866–874, Mar. 2007.

[21] D. R. Brillinger, *Time Series: Data Analysis and Theory*. New York, NY, USA: Holt, Rinehart and Winston, 1975.

[22] T. C. Lystig and J. P. Hughes, "Exact computation of the observed information matrix for hidden Markov models," *J. Comput. Graph. Statist.*, vol. 11, no. 3, pp. 678–689, 2002.

[23] C. J. Willy, W. J. J. Roberts, and T. A. Mazzuchi, "Recursions for the MMPP score vector and observed information matrix," *Stochastic Models*, vol. 26, no. 4, pp. 649–665, Jul. 2010.

[24] T. Nguyen, "Hidden Markov model based spectrum sensing for cognitive radio," Ph.D. dissertation, Dept. Elect. Comput. Eng., George Mason Univ., Fairfax, VA, USA, Apr. 2013.

[25] Shared Spectrum Company, "General survey of radio frequency bands—30 MHz to 3 GHz," Shared Spectrum Company, Vienna, VA, USA, Tech. Rep., Aug. 2010. [Online]. Available: http://www.sharedspectrum.com

Yuandao Sun (S'15) received the Ph.D. degree in electrical and computer engineering from George Mason University, in 2015, and the M.S. degree in electrical and computer engineering from Tongji University, in 2011. In 2015, he joined Deloitte Consulting LLP, where he is currently a Data Scientist. His current research interests include cognitive radio networks, signal processing, data mining, and machine learning.

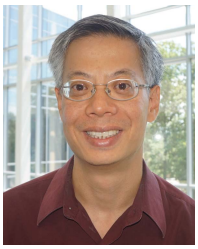

Brian L. Mark (S'91–M'95–SM'08) received the B.A.Sc. degree in computer engineering with an option in mathematics from the University of Waterloo, in 1991, and the Ph.D. degree in electrical engineering from Princeton University, in 1995. He was a Research Staff Member at C&C Research Laboratories, NEC USA from 1995 to 1999. In 1999, he was on part-time leave from NEC as a Visiting Researcher with the École Nationale Supérieure des Télécommunications, Paris, France. In 2000, he joined George Mason University, where he currently is a Professor of electrical and computer engineering. He served as the Acting Chair of the Department of Bioengineering from 2015 to 2016. His research interests lie in the design and performance analysis of communication networks. He was an Associate Editor of the IEEE TRANSACTIONS ON VEHICULAR TECHNOLOGY from 2006 to 2009.

Yariv Ephraim (S'82–M'84–SM'90–F'94) received the D.Sc. degree in electrical engineering from the Technion–Israel Institute of Technology, Haifa, Israel, in 1984. From 1984 to 1985, he was a Rothschild Post-Doctoral Fellow at the Information Systems Laboratory, Stanford University, Palo Alto, CA. From 1985 to 1993, he was a Member of Technical Staff at the Information Principles Research Laboratory, AT&T Bell Labs, Murray Hill, NJ. In 1991, he joined George Mason University, Fairfax, VA, where he currently is a Professor of electrical and computer engineering. His research interests are in statistical signal processing.